Flexible and Reliable UAV-Assisted Backhaul Operation in 5G mmWave Cellular Networks

Margarita Gapeyenko, Vitaly Petrov, Dmitri Moltchanov,
Sergey Andreev, Nageen Himayat, and Yevgeni Koucheryavy

Abstract—To satisfy the stringent capacity and scalability requirements in the fifth generation (5G) mobile networks, both *wireless access and backhaul links* are envisioned to exploit millimeter wave (mmWave) spectrum. Here, similar to the design of access links, mmWave backhaul connections must also address many challenges such as multipath propagation and dynamic link blockage, which calls for advanced solutions to improve their reliability. To address these challenges, 3GPP New Radio (NR) technology is considering a *flexible* and *reconfigurable* backhaul architecture, which includes dynamic link rerouting to alternative paths. In this paper, we investigate the use of aerial relay nodes carried by e.g., *unmanned aerial vehicles* (UAVs) to allow for such dynamic routing, while mitigating the impact of occlusions on the terrestrial links. This novel concept requires an understanding of mmWave backhaul dynamics that accounts for: (i) realistic 3D multipath mmWave propagation; (ii) dynamic blockage of mmWave backhaul links; and (iii) heterogeneous mobility of blockers and UAV-based assisting relays. We contribute the required mathematical framework that captures these phenomena to analyze the mmWave backhaul operation in characteristic urban environments. We also utilize this framework for a new assessment of mmWave backhaul performance by studying its spatial and temporal characteristics. We finally quantify the benefits of utilizing UAV assistance for more reliable mmWave backhaul. The numerical results are confirmed with 3GPP-calibrated simulations, while the framework itself can aid in the design of robust UAV-assisted backhaul infrastructures in future 5G mmWave cellular.

Index Terms—5G New Radio; millimeter wave; multipath 3D channel model; UAV communications; integrated access and backhaul; dynamic human body blockage; moving cells.

I. INTRODUCTION

Over the past years, the work on fifth-generation (5G) networks has achieved impressive results [1], [2]. 3GPP has recently ratified non-standalone 5G New Radio (NR) technology to augment further LTE evolution. Currently, the standardization has completed the standalone 5G NR specifications to allow for independent NR-based deployments [3]. Catering for high-rate and reliable wireless connectivity, the 5G cellular paradigm aims to densify the network with terrestrial base stations [4] by additionally employing moving (e.g., car-mounted) small cells for on-demand capacity boost as well as harnessing more abundant millimeter-wave (mmWave) spectrum for both access and backhaul radio links [5], [6].

M. Gapeyenko, V. Petrov, D. Moltchanov, S. Andreev, and Y. Koucheryavy are with Tampere University of Technology, Tampere, Finland (e-mail: {firstname.lastname, evgeni.koucheryavy}@tut.fi).

N. Himayat is with Intel Corporation, Santa Clara, CA, USA (e-mail: nageen.himayat@intel.com).

Despite the notable benefits of the mmWave band, it also poses new challenges due to highly directional mmWave links subject to complex multipath propagation, which is susceptible to link blockage phenomena because of a wide range of obstacles [7]–[9]. There has been a surge in research work on reliability analysis of mmWave access to outline techniques for mitigating the inherent limitations of mmWave-based communication [10]–[14].

As that work matures, provisioning of high-rate backhaul capabilities for 5G has attracted recent attention, as mmWave backhaul links remain vulnerable to similar blockage issues [15]. Aiming to assess and improve reliability of mmWave backhaul operation in 5G NR systems, 3GPP has initiated a new study on integrated access and backhaul, which specifies the respective challenges and requirements. The panned specifications target to construct a flexible and reconfigurable system architecture with dynamic backhaul connections. In this context, the capability to reroute backhaul links in case of their blockage by moving humans and car bodies becomes essential [16]. Extending the 3GPP studies on the matter, the utilization of unmanned aerial vehicles (UAVs) equipped with radio capabilities and acting as mobile relay nodes may be considered to further improve flexibility and reliability of backhaul operation.

The recent acceleration in user traffic fluctuations calls for more flexible and reliable backhaul solutions in 5G mmWave cellular, which may require dynamic rerouting. Therefore, the integration of both terrestrial and aerial network components to achieve this goal is essential. The corresponding performance assessment requires an appropriate evaluation methodology that may capture the dynamics of backhaul links, mmWave radio propagation properties, and blockage phenomena caused by moving objects. Different from mmWave access, the research literature on 5G mmWave backhaul is scarce. In [17], the authors propose an analytical model for coexistence of access and backhaul links, while in [18] the capacity evaluation of cellular networks with in-band wireless backhaul was proposed. In [19], a performance evaluation of mmWave backhaul links is conducted.

To the best of our knowledge, an integrated methodology for flexible mmWave backhaul operation with dynamic links that reroute subject to the channel conditions has not been available as of yet. Addressing that gap, this work offers a new methodology that can assess complex scenarios with multiple terrestrial and aerial base stations. These are equipped with mmWave backhaul capabilities and can reroute their links to maintain uninterrupted connectivity over unreliable blockage-prone channels, while leveraging UAV-based relay assistance as illustrated in Fig. 1.

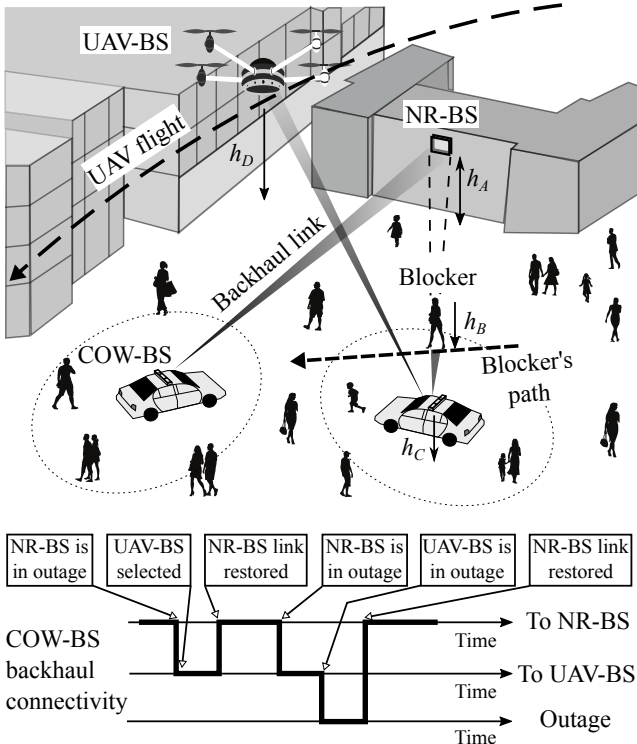Our considered scenario captures three important compo-

Fig. 1. Scenario of interest with UAV-BS assistance.

nents of future 5G mmWave backhaul solutions: (i) dynamic blockage of mmWave links; (ii) complex multipath propagation in urban environments; and (iii) flexible mobility of assisting UAV relays. A range of simpler scenarios can also be assessed by applying the relevant components of our developed framework with opportunistic UAV mobility model (e.g., those with static deployment of UAV-based relays [20]–[22]). The contributions of this work are therefore as follows.

- A novel mathematical framework that captures the essential features of mmWave backhaul operation under dynamic blockage by moving humans as well as possible link rerouting to UAV-based relay nodes in realistic scenarios under 3D multipath propagation. This analytical framework is further verified with detailed system-level simulations (SLS) that explicitly model the 3GPP 3D multipath propagation channel.

- A performance assessment of flexible mmWave backhaul operation in crowded urban deployments that includes both time-averaged and time-dependent metrics of interest, such as outage probability and spectral efficiency together with outage and non-outage duration distributions. A highlight of our methodology is characterization of uninterrupted connectivity duration, which accounts for tolerable outage time subject to application-specific requirements.

- An understanding of benefits made available with UAV relay assistance to mmWave backhaul reliability in realistic city scenarios. We demonstrate that under certain speed, intensity, and service capacity, the use of UAV-based relays enables significant gains for the system performance. In particular, outage probability and outage duration in the considered scenario become notably reduced, while spectral efficiency increases substantially.

The rest of this text is organized as follows. In Section II,

our system model of the target urban scenario is introduced. The analytical framework for time-averaged performance evaluation of mmWave backhaul operation is outlined in Section III. Further, an analytical model to assess temporal metrics of interest in mmWave backhaul is contributed by Section IV. The corresponding numerical results that explore the spatial and temporal characteristics of flexible mmWave backhaul by leveraging assistance of UAV relay nodes are offered in Section V. Conclusions are drawn in the last section.

II. System Model

A. Network deployment and COW-BSs

We consider a circular area with the radius of R, where several *"Cell on Wheels"* base stations (COW-BSs) are distributed uniformly according to a Poisson Point Process (PPP) with the density of λ_C. These COW-BSs provide connectivity to the human users in their vicinity and are equipped with mmWave backhaul links to the terrestrial New Radio base stations (NR-BSs) as well as aerial UAV-carried base stations (UAV-BSs) as illustrated in Fig. 2. In the scenarios where over-provisioning leads to increased operator expenses (e.g., temporary and unexpected events), on-demand network densification with COW-BSs might become a viable option. The height of a COW-BS is h_C. A terrestrial NR-BS is located at the circumference of the circle area at the height of h_A. Since the height of a consumer vehicle is generally lower than that of a pedestrian, the latter may act as a potential blocker to the mmWave signal [23]. We assume that walking pedestrians form a PPP with the density of λ_B and the height of h_B, where $h_A > h_B > h_C$.

The human blockers in our scenario are *dynamic* and their travel patterns are assumed to follow the Random Direction Mobility (RDM) model. The angle of movement in this formulation is chosen uniformly within $[0, 2\pi)$, while the time of travel until the subsequent turn is distributed exponentially. The UAV-BSs may fly through the center of the circle by entering and leaving it at random points that are distributed uniformly across its circumference [24]. This work considers
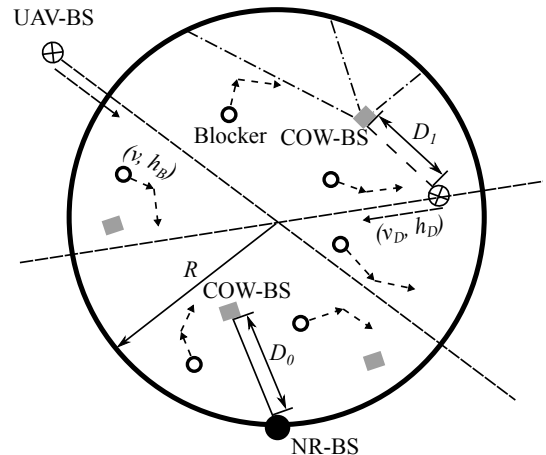

Fig. 2. Geometrical 2D illustration of target setup.

mobility of the UAV-BS as it becomes a distinguishing feature for this new type of BSs. In [25], the authors demonstrate the benefits of dynamic over static UAV deployments. Therefore, mobility modeling is important to assess system-level performance in the scenarios where several types of BSs may coexist. The speed of the UAV-BSs is v_D and their altitude is h_D. The process of entering the circle by the UAV-BSs is assumed to be Poisson in time with the intensity of λ_D. The remaining important notation is summarized in Table I.

B. 3D channel model and dynamic blockage of backhaul links

In order to model the mmWave backhaul links, we employ the current 3GPP 3D multipath channel model [11] by taking into account all of the key features of mmWave communication. The model assumes that there are multiple alternative paths (named *clusters*) between the Tx and the Rx (see Fig. 3), each featured by its own delay, pathloss, and zenith of arrival/departure angles. Each of these paths can be blocked or non-blocked by the moving human blockers using the analytical model from [8].

The COW-BSs utilize beamsteering mechanisms to always use the *best* path, which is currently non-blocked and has the strongest signal. Beamsteering employed at all the communicating nodes also minimizes the level of interference between the backhaul links, thus making the considered mmWave regime noise-limited [26]. Signal blockage by buildings is not modeled, as none occlude the backhaul links between the COW-BSs and the NR-BSs/UAV-BSs in the target scenario.

While the employed 3GPP model is sufficiently detailed and accurate [27], the complexity of the used algorithms [11] challenges its analytical tractability. Therefore, in our mathematical study, we utilize a statistical approximation of the key modeling parameters [28], such as power of every cluster transmitted by the NR-BS and the UAV-BS, $P_{A,i}$ and $P_{D,i}$, and zenith angle of arrival (ZOA) for every cluster, $\theta_{A,i}$ and $\theta_{D,i}$, where $i = 1, 2, \ldots, N$ is the cluster number.

C. mmWave backhaul connectivity model

The radio channel conditions of the backhaul links are dynamic in nature due to temporal variations of the propagation environment. These are captured by the utilized propagation model [28], while the mobility of human blockers surrounding the COW-BSs is modeled explicitly in our work. The NR-BS is assumed as the primary option for the backhaul links of COW-BSs (see Fig. 1). When COW-BS is currently in outage
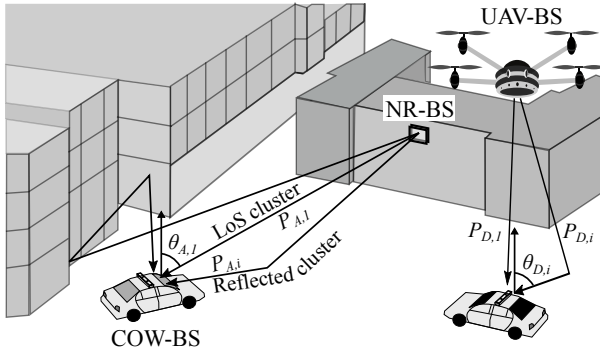

Fig. 3. 3GPP-driven 3D multipath channel model.

TABLE I
SUMMARY OF NOTATION AND PARAMETERS

Notation	Description
Deployment	
h_A, h_C, h_D	Heights of NR-BS, COW-BS, UAV-BS
λ_C, λ_B	Density of COW-BSs and blockers per unit area
r_B, v, h_B	Radius, speed, and height of a blocker
R	Radius of the service area
λ_D	Temporal intensity of UAV-BSs entering the service area
T_D, v_D	Time and speed of UAV-BSs traversing the service area
K_D	UAV-BS service capacity
Technology	
N	Number of 3D multipath propagation clusters
$\theta_{A,i}$ and $\theta_{D,i}$	ZOA of i-th cluster from NR-BS and UAV-BS
$f_{\theta_{A,i}}$ and $f_{\theta_{D,i}}$	Pdf of ZOA of i-th cluster from NR-BS and UAV-BS
C and $E[C]$	Spectral efficiency and its mean value
p_O	Outage probability
Δ_O	Tolerable outage duration
T_U and $E[T_U]$	Uninterrupted connectivity time and its mean value
Mathematical framework	
$p_{D,av}$	Probability of UAV-BS availability
P_A and P_D	Received power at NR-BS to COW-BS and UAV-BS to COW-BS links
f_{P_A} and f_{P_D}	Pdf of received power at NR-BS to COW-BS and UAV-BS to COW-BS links
$f_{P_{A,i}}$ and $f_{P_{D,i}}$	Pdf of power of i-th cluster arriving from NR-BS and UAV-BS
u_n	Pmf of number of UAV-BSs available for COW-BS
$p_{A,i}$ and $p_{D,i}$	Blockage probability of i-th cluster arriving from NR-BS and UAV-BS
$\lambda_{B,T}$	Temporal intensity of blockers crossing the blockage zone
T_B and L_B	Time and distance walked inside the blockage zone by a single blocker
f_η, f_ω	Pdf of blocked and unblocked intervals
f_O and f_G	Pdf of outage and non-outage duration

with respect to NR-BS (i.e., the signal received from NR-BS is too weak), COW-BS may temporarily reroute its backhaul traffic to UAV-BS traversing the area. Once the radio link to NR-BS recovers, COW-BS reconnects to the terrestrial NR-BS and reroutes its backhaul traffic back to it. Hence, the UAV-BSs are employed in unfavorable conditions to improve the continuity of backhaul links.

We measure the capacity of UAV-BS in terms of the maximum number of simultaneously supported backhaul links, which we denote as K_D. This consideration reflects the potential limitations of the mmWave radio equipment carried by the UAV-BS as well as the specifics of the employed network architecture and connectivity protocols. In its turn, the connection between the UAV-BS and the core network is inherently characterized by unobstructed line-of-sight propagation without obstacles [29]. Therefore, this link is modeled as always reliable.

D. Illustrative metrics of interest

To assess the performance quality of the mmWave backhaul links in the described scenario, we concentrate on two types of metrics, namely, time-averaged and time-dependent. In the former case, we address (i) outage probability, p_O, and (ii) spectral efficiency, C. In the latter, we assume that the system may tolerate a certain fixed outage duration Δ_O and thus derive (iii) the mean uninterrupted connectivity time, $E[T_U]$. As intermediate parameters, we also obtain (iv) the outage and non-outage duration distributions, f_O and f_G, respectively.

III. TIME AVERAGED ANALYSIS

In this section, we address the time-averaged system metrics, including outage probability and spectral efficiency.

A. Outage Probability

The outage probability p_O for a randomly chosen COW-BS in the area of interest is obtained as follows. Observe that the COW-BS is always associated with the NR-BS when the latter is in non-outage conditions. Otherwise, the COW-BS is connected to a randomly chosen UAV-BS that is available, provided that there is at least one UAV-BS in non-outage conditions having fewer than K_D COW-BSs connected to it. Hence, the outage probability is produced as

$$p_O = p_{A,O}(u_0 + (1 - u_0)(u_{0,n} + (1 - u_{0,n})p_{D,nav})), \quad (1)$$

where u_0 is the probability of having no UAV-BS traversing the area at the moment, $u_{0,n}$ is the probability of having no UAV-BS in non-outage conditions, $p_{A,O}$ and $p_{D,nav}$ are the outage probability on the COW-BS to NR-BS link and the probability that the UAV-BS is currently unavailable, respectively. In what follows, we derive these unknown terms.

1) Outage probability on COW-BS to NR-BS and COW-BS to UAV-BS links: Consider a randomly chosen COW-BS. Let $p_{A,i}$ be the probability that i-th cluster between the NR-BS and the COW-BS is blocked and first consider blockage of the LoS path, $p_{A,1}$. Fixing the distance x between NR-BS and COW-BS, we observe that there is always a so-called *blockage zone* as shown in Fig. 4. At any given instant of time t, the number of blockers moving according to the RDM model within the service zone follows a Poisson distribution [30]. Hence, the probability that the LoS path is blocked is given by

$$p_{A,1}(x) = 1 - e^{\left(-2\lambda_B r_B \left[x \frac{h_B - h_C}{h_A - h_C} + r_B\right]\right)}. \quad (2)$$

Let D_0 be a random variable (RV) denoting the 2D distance between the NR-BS and a randomly chosen COW-BS, and let $f_{D_0}(x)$ be its probability density function (pdf). Noticing that the COW-BSs are uniformly distributed within a service area circle, the sought distance is [31]

$$f_{D_0}(x) = \frac{2x}{\pi R^2} \cos^{-1}\left(\frac{x}{2R}\right), 0 < x < 2R. \quad (3)$$
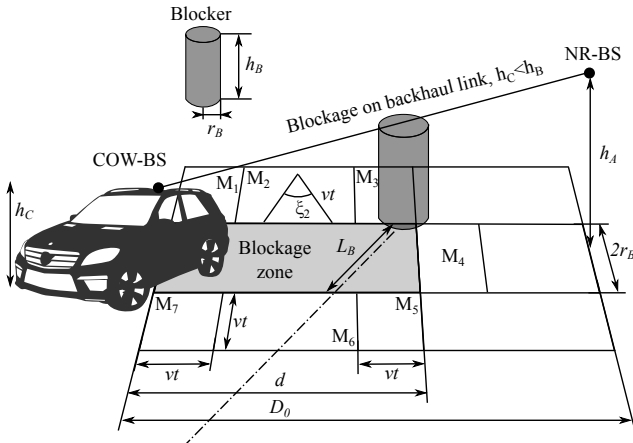

Fig. 4. Illustration of dynamic blockage process.

The LoS path blockage probability is then

$$p_{A,1} = \int_0^{2R} f_{D_0}(x) p_{A,1}(x) dx. \quad (4)$$

Consider now the blockage probability for i-th cluster, $i = 2, 3, \ldots, N$. As opposed to the LoS path, the 3GPP model does not explicitly specify where the reflected cluster comes from. Instead, it provides the ZOA, $\theta_{A,i}$ and $\theta_{D,i}$, $i = 2, 3, \ldots, N$. In [28], it was shown that the ZOA for all clusters follows a Laplace distribution and we denote it as the pdf $f_{\theta_{A,i}}(y; x)$.

The blockage probability $p_{A,i}(x)$ of every cluster is then

$$p_{A,i} = \int_{-\pi}^{\pi} \int_0^{2R} f_{\theta_{A,i}}(y; x) p_{A,i}(y) dx dy, \quad (5)$$

where $p_{A,i}(y)$ is the blockage probability as a function of the ZOA, derived as

$$p_{A,i}(y) = 1 - e^{[-2\lambda_B r_B(\tan y(h_B - h_C) + r_B)]}. \quad (6)$$

Substituting (6) and pdf of ZOA from [28], we obtain

$$p_{A,i} = \int_{-\pi}^{\pi} \int_0^{2R} \frac{1 - e^{-2\lambda_B r_B(\tan y(h_B - h_C) + r_B)}}{2b_z e^{\frac{y - a_z(x)}{b_z}}} dx dy, \quad (7)$$

where $a_z(x) = \frac{\pi}{2} - \arctan\left(\frac{h_A - h_C}{x}\right)$ and b_z, $z = 2, 3, \ldots, N$, are the parameters estimated from the statistical data (see [28] for details) and b_z is given as

$$b_1 = 0, b_2 = 0.3146, b_3 = 0.3529, b_4 = 0.4056, b_5 = 0.4897. \quad (8)$$

After characterizing the blockage probabilities of individual clusters on the COW-BS to NR-BS link, we derive an expression for the received power. As shown in [28], the fraction of power of i-th cluster between the NR-BS and the COW-BS separated by the distance of x follows a Log-normal distribution with the pdf $f_{P_{A,i}}(y; x)$.

Once the fraction of power distributions is obtained, the received power from every cluster is calculated as

$$P_{A,z} = P_{s,z} 10^{(P_T - 30 - L)/10}, z = 1, 2, \ldots, \quad (9)$$

where P_T is the transmit power in dBm and L is the path loss in dB. Then, $P_{A,z}$ is given as

$$P_{A,z} = P_{s,z} 10^{(A_p - 21.0 \log_{10}(D_{3,0}))/10}, \quad (10)$$

where $A_p = P_T - 30 - 32.4 - 20 \log_{10} f_c$.

As one may observe, $P_{A,z}$ is a function of two RVs, $P_{s,z}$ and $D_{3,0}$, and $f_{D_{3,0}}(x)$ is the pdf of the 3D distance between the NR-BS and the COW-BS in the form

$$f_{D_{3,0}} = \frac{2x}{\pi R^2} \cos^{-1}\left(\frac{\sqrt{x^2 - (h_A - h_C)^2}}{2R}\right), \quad (11)$$

where $x \in (h_A - h_C, \sqrt{4R^2 + (h_A - h_C)^2})$.

Since $D_{3,0}$ and $P_{s,z}$ are independent, their joint pdf is

$$f_{P_{s,z}, D_{3,0}}(x_1, x_2) = \frac{1}{x_1 d_z \sqrt{2\pi}} e^{\left(-\frac{(\ln x_1 - c_z)^2}{2d_z^2}\right)} \times$$
$$\frac{2x_2}{\pi R^2} \cos^{-1}\left(\frac{\sqrt{x_2^2 - (h_A - h_C)^2}}{2R}\right), \quad (12)$$

where c_z and d_z, $z = 2, 3, \ldots$, are the parameters derived from the statistical data (see [28] for details) and given as

$$c_1 = -2.88, c_2 = -3.55, c_3 = -4.1, c_4 = -4.98, c_5 = -6.2,$$
$$d_1 = 1.2, d_2 = 1.1, d_3 = 1.3, d_4 = 1.8, d_5 = 2.51. \quad (13)$$

Finally, the pdf of $P_{A,z}$ is

$$f_{P_{A,z}}(y) = \int_{x_{2,\min}}^{x_{2,\max}} f_{P_{s,z}, D_{3,0}} \left(\frac{y}{10^{(A_p - 21.0 \log_{10}(x_2))/10}}, x_2 \right) \times$$
$$\frac{1}{10^{(A_p - 21.0 \log_{10}(x_2))/10}} dx_2, \quad (14)$$

where $x_{2,\min} = h_A - h_C$ and $x_{2,\max} = \sqrt{4R^2 + (h_A - h_C)^2}$.

Assuming mutual independence in the cluster blockage, the pdf of the received power is produced as

$$f_{P_A}(y) = \sum_{k=1}^{N} \left[(1 - p_{A,k}) \prod_{j=1}^{k-1} p_{A,j} \right] f_{P_{A,k}}(y), \quad (15)$$

where the weights are the probabilities of choosing cluster i.

Finally, the outage probability with the NR-BS is

$$p_{A,O} = Pr\{P_A(y) \le N_0 T_S\} = \int_0^{N_0 T_S} f_{P_A}(y) dy, \quad (16)$$

where N_0 is the Johnson-Nyquist noise at the receiver and T_S is the SNR threshold. Note that due to the complex structure of the conditional received power $f_{P_A}(y)$, the outage probability $p_{A,O}$ can only be produced with numerical integration.

The LoS path and i-th cluster blockage probability on a link between the UAV-BS and the COW-BS are obtained similarly except for the 2D distance between UAV-BS and COW-BS, D_1, with the pdf given as

$$f_{D_1}(x) = \frac{4x}{\pi R^2} \left[\cos^{-1} \left(\frac{x}{2R} \right) - \frac{x}{2R} \sqrt{1 - \frac{x^2}{4R^2}} \right], \quad (17)$$

where $x \in (0, 2R)$. Using this result, the corresponding 3D distance between the UAV-BS and the COW-BS constitutes

$$f_{D_{3,1}} = \frac{4x}{\pi R^2} \left[\cos^{-1} \left(\frac{\sqrt{x^2 - (h_D - h_C)^2}}{2R} \right) - \right.$$
$$\left. - \frac{\sqrt{x^2 - (h_D - h_C)^2}}{2R} \sqrt{1 - \frac{x^2 - (h_D - h_C)^2}{4R^2}} \right], \quad (18)$$

where $x \in (h_D - h_C < x < \sqrt{4R^2 + (h_D - h_C)^2})$.

2) Availability probability of UAV-BS: To complete the derivation of p_O, we find the probability that at least one UAV-BS in non-outage conditions is available for service, $p_{D,av}$.

The time spent by each UAV-BS within the service area is constant and equals $T_D = 2R v_D$, where v_D is the speed of UAV-BS. Hence, the number of UAV-BSs that are available in the service zone is captured by the $M/G/\infty$ queuing system with a constant service time. It is known that the number of customers in $M/G/\infty$ queue coincides with the number of customers in $M/M/\infty$ queue and follows a Poisson distribution with the parameter $\lambda_D T_D$ [32][1].

---

[1]To ensure a certain number of UAV-BSs above the area one may directly use a mean number of UAV-BSs.

Note that the availability of UAV-BSs is not sufficient for the COW-BS to be able to associate with them. In addition, there should be at least one UAV-BS in non-outage conditions. The intensity of such UAV-BSs is $\lambda_D T_D (1 - p_{D,O})$, where $p_{D,O}$ is the probability that a randomly selected UAV-BS resides in the outage conditions. Therefore, the number of UAV-BSs that are available for the COW-BS U follows a Poisson distribution with the probability mass function (pmf) of

$$u_n = \frac{[\lambda_D T_D (1 - p_{D,O})]^n}{n!} e^{-\lambda_D T_D (1 - p_{D,O})}, \quad (19)$$

where $n = 0, 1, \ldots$.

Let W denote the number of COW-BSs in the outage conditions. The number of COW-BSs in the service area follows a Poisson distribution with the density of λ_C. Hence, the number of COW-BSs in the outage conditions also follows a Poisson distribution with the parameter of $\lambda_C p_{A,O} \pi R^2$. The probability that the UAV-BS remains available for service is

$$p_{D,av} = Pr\{K_D U - W > 0\} = \sum_{i=1}^{\infty} Pr\{Z = i\}, \quad (20)$$

where $Z = K_D U - W$.

Observe that $K_D U$ is a scaled Poisson RV in (21), which implies that $p_{D,av}$ can be evaluated numerically for any value of K_D. The pmf of Z is then established as

$$Pr\{Z = z\} = \sum_{x=0}^{\infty} \frac{|K_D x - 1|}{K_D} \frac{[\lambda_C p_{A,O} \pi R^2]^{(K_D x - z)}}{(K_D x - z)!} \times$$
$$e^{\left(-\lambda_C p_{A,O} \pi R^2 - \lambda_D T_D (1 - p_{D,O}) \right)} \frac{[\lambda_D T_D (1 - p_{D,O})]^{x/K_D}}{(x/K_D)!}. \quad (21)$$

B. Spectral efficiency

Consider now spectral efficiency of an arbitrarily chosen COW-BS. Observe that this COW-BS spends a fraction of time, p_A, connected to the NR-BS and a fraction of time, p_D, connected to the UAV-BS. The rest of the time, p_O, this COW-BS resides in outage. Hence, the spectral efficiency is

$$C = p_A \log_2 \left[1 + \frac{P_A}{N_0} \right] + p_D \log_2 \left[1 + \frac{P_D}{N_0} \right], \quad (22)$$

where P_A and P_D are the received powers whenever associated with NR-BS and UAV-BS.

Observe that $p_{A,O} = 1 - p_A$ is the outage probability when only NR-BS is available. Recalling that UAV-BS are only employed when the NR-BS to COW-BS link experiences outage conditions, the fraction of time that the COW-BS is associated with the UAV-BS is $p_D = p_{A,O} p_{D,av}$. Therefore, the mean spectral efficiency is provided by

$$E[C] = (1 - p_{A,O}) \int_0^{\infty} f_{P_A}(x) \log_2 \left[1 + \frac{P_A}{N_0} \right] dx +$$
$$+ p_{A,O} p_{D,av} \int_0^{\infty} f_{P_D}(x) \log_2 \left[1 + \frac{P_D}{N_0} \right] dx, \quad (23)$$

which can be evaluated numerically.

In addition to the mean value, the form of (22) enables us to determine the distribution of the spectral efficiency. Observe that the spectral efficiencies associated with the UAV-BS to

COW-BS and the NR-BS to COW-BS links are independent RVs. The resulting pdf takes the following form

$$f_C(x) = \begin{cases} \int_0^\infty \dfrac{(2^{f_{P_A}(y)} - 1)(2^{f_{P_A}(x-y)} - 1)}{(N_0^4 2^x \log^2 2)^{-1}} dy, \ x > 0, \\ p_O, \ x = 0, \end{cases} \quad (24)$$

where the convolution integral can be evaluated numerically.

IV. TIME DEPENDENT ANALYSIS

In this section, we continue by quantifying uninterrupted connectivity performance, including the outage and non-outage duration distributions as well as the uninterrupted connectivity duration.

A. Dynamics of cluster blockage process

To capture the temporal dynamics of the blockage process for a single cluster, we need to track the blockers that are crossing the blockage zone, see Fig. 4. We begin by considering the dynamics of the LoS blockage process and concentrate on the temporal properties of the process when the blockers are entering the blockage zone and occluding the LoS.

We specify the area around the blockage zone as shown in Fig. 4, where the moving blockers may cross the blockage zone by occluding the LoS between the COW-BS and the NR-BS. To specify these conditions, the area around the blockage zone is further divided into i, $i = 1, 2, ...7$, zones. The intensity of blockers crossing the blockage zone of the COW-BS located at the distance of x from the NR-BS is approximated as

$$\lambda_{B,T}(z) = \sum_{i=1}^7 \iint_{M_i} \frac{g_i(x,y) Pr\{A_B\} Pr\{T_B > t\}}{(\lambda_B M_i)^{-1}} dx dy, \quad (25)$$

where the event A_B is when a blocker moves towards the blockage zone (see Fig. 4), M_i is the area of zone i, $g_i(x,y)$ is the pdf of the blocker locations in zone i. Here, $g_i(x,y) = 1/M_i$ as the blockers move according to the RDM model and at every instant of time their coordinates are distributed uniformly within the area [30], while $Pr\{T_B > t\} = e^{-1/E[\tau]}$ is the probability that such movement is longer than t seconds.

Observe that the probability for a blocker to move towards CDEF is $Pr\{A_B\} = \xi_i(x,y)/2\pi$, where $\xi_i(x,y)$ is a range of movement angles within zone i that lead to crossing the blockage zone. We thus simplify (25) as

$$\lambda_{B,T}(z) = \frac{\lambda_B e^{-1/E[\tau]}}{2\pi} \sum_{i=1}^7 \iint_{M_i} \xi_i(x,y) \, dx \, dy, \quad (26)$$

where $\xi_i(x,y)$ are calculated as

$$\xi_1(x,y) = \xi_3(x,y) = \xi_5(x,y) = \xi_7(x,y) = \cos^{-1}\left(\frac{x}{vt}\right) + \tan^{-1}\left(\frac{y}{x}\right),$$
$$\xi_2(x,y) = \xi_6(x,y) = 2\cos^{-1}(x/vt),$$
$$\xi_4(x,y) = 2\tan^{-1}(x/y), \quad (27)$$

and $M_1 = M_3 = M_5 = M_7$ with x-coordinate within the range of $(0, vt)$ and y-coordinate within the range of $(0, vt/2)$, $M_2 = M_6$ with x-coordinate within the range of $(0, vt)$ and y-coordinate within the range of $(0, d - 2vt)$, M_4 with x-coordinate within the range of $(0, 2r_B)$ and y-coordinate within the range of $(0, vt)$, where $2r_B < vt$.

It has been shown in [33] that the process of meetings between a stationary node and a node moving inside a bounded area according to the RDM is approximately Poisson. We build on this result to approximate the nature of the process of blockers meeting the blockage zone. Due to the properties of the RDM model, the entry point is distributed uniformly over the three sides of the blockage zone [30].

Let η and ω be the RVs denoting the blocked and non-blocked periods, respectively. Since blockers enter the zone in question according to a Poisson process with the intensity of $\lambda_{B,T}(x)$, the time spent in the unblocked part, ω, follows an exponential distribution with the parameter of $\lambda_{B,T}(x)$, $F_\omega(t;x) = 1 - e^{-\lambda_{B,T}(x)t}$, as demonstrated in [8]. The pdf of η, $f_\eta(t;x)$, is the same as the distribution of the busy period in the $M/GI/\infty$ queuing system [34] given by (28), where F_{T_B} is the CDF of time that one blocker spends in the blockage zone, which is provided in [8].

The pdfs of the blocked and non-blocked intervals, $f_\eta(t;x)$ and $f_\omega(t;x)$, are conditioned on the distance between COW-BS and NR-BS. Deconditioning with (3), we obtain the pdfs of the blocked and non-blocked intervals when associated with the NR-BS as

$$f_\eta(t) = \int_0^{2R} f_\eta(t;x) f_{D_0}(x;R) dx,$$
$$f_\omega(t) = \int_0^{2R} f_\omega(t;x) f_{D_0}(x;R) dx, \quad (29)$$

which can be calculated numerically.

To capture the dynamics of the cluster blockage process, we can represent it by using a continuous-time Markov chain (CTMC) process with two states, which is defined by the infinitesimal generator in the following form

$$\Lambda_{1,A} = \begin{bmatrix} -\alpha_{1,A} & \alpha_{1,A} \\ \beta_{1,A} & -\beta_{1,A} \end{bmatrix}, \quad (30)$$

where the subscript $(1, A)$ shows that the model is built for the LoS cluster of the NR-BS to COW-BS link, while $\alpha_{1,A} = 1/E[\eta]$ and $\beta_{1,A} = 1/E[\omega]$ are the means of blocked and non-blocked intervals of the LoS cluster given in (29).

The process of blockage for other clusters on the NR-BS to COW-BS link is analyzed similarly. The key difference is that the blockage zone is specified by the ZOA instead of the heights of NR-BS and COW-BS as well as the distance between them. Let us denote the generators of all clusters associated with the NR-BS to COW-BS link by $\Lambda_{i,A}$, $i = 1, 2, \ldots, N$. Assuming independence between the cluster blockage processes, the associated CTMC model, $\{S_A(t), t > 0\}$, $S_A(t) \in \{1, 2, \ldots, 2^N\}$, is a superposition of the individual blockage processes. The infinitesimal generator of $\{S_A(t), t > 0\}$ is then given by the Kronecker product of $\Lambda_{i,A}$, $i = 1, 2, \ldots, N$.

The blockage dynamics of the UAV-BS to COW-BS link is represented similarly by leading to the Markov process approximation $\{S_D(t), t > 0\}$, $S_D(t) \in \{1, 2, \ldots, 2^N\}$. Finally, the aggregate blockage model of both links is represented by a superposition of the blockage processes that characterize the NR-BS to COW-BS and the UAV-BS to COW-BS links. The resulting infinitesimal generator is $\Lambda = \Lambda_A \otimes \Lambda_D$.

$$F_\eta(x) = 1 - \left[[1 - F_{T_B}(x)] \left[1 - \int_0^x (1 - F_\eta(x-z)) \exp(-\lambda_{B,T} F_{T_B}(z)) \lambda_{B,T} dz \right] + \int_0^x (1 - F_\eta(x-z)) |de^{-\lambda_{B,T} F_{T_B}(z)}| \right]. \quad (28)$$

B. Performance measures of interest

1) Outage and non-outage duration distribution: Having the CTMC representation of the outage process, we can now calculate time-dependent performance metrics of interest, including the distributions of consecutive intervals spent in outage and non-outage conditions, the corresponding distributions of residual time, as well as the distribution and the mean duration of uninterrupted connectivity.

Let RVs G and O denote the non-outage and outage time durations, respectively. The distribution of time spent in outage, $f_O(x)$, $x > 0$, is directly given by the sojourn time in the state where all clusters are blocked. For our model, it is always state 1. The distribution of time spent in the non-outage state can be found by modifying the CTMC to have an absorption state in outage. Then, the sought distribution is the first-passage time (FPT) to the outage state that can be established by using [35]. Particularly, let $f_G(t)$ be the pdf of the FPT from the set of non-blockage states, $\{2, 3, \ldots, 2 \times 2^N\}$, to the blockage state.

It is easy to see that the sought distribution is of the phase-type nature [36] with the representation $(\vec{\alpha}, S)$, where $\vec{\alpha}$ is the initial state distribution defined over $\{2, 3, \ldots, 2 \times 2^N\}$ and S is obtained from the infinitesimal generator Λ by excluding the first row and column. The pdf is then given by [37] as

$$f_G(t) = \vec{\alpha} e^{St} \vec{s}_0, \ t > 0, \quad (31)$$

where $\vec{s}_0 = -S\vec{1}$, $\vec{1}$ is the vector of ones with size $2^N - 1$, while e^{St} is the matrix exponential defined as $e^{St} = \sum_{k=0}^\infty \frac{1}{k!} (St)^k$.

The initial state distribution, $\vec{\alpha}$, is determined by the normalized rates out of the outage state e.g.,

$$\alpha_i = \begin{cases} 0, & i = 1, \\ \pi_i / \sum_{j=2}^{2^N} \pi_j, & i = 2, 3, \ldots, 2^N. \end{cases} \quad (32)$$

2) Uninterrupted connectivity time: Consider now an application that may tolerate at most Δ_O in the outage conditions, which implies that all of the outages whose durations are less than Δ_O do not cause connectivity interruptions. The probability that a session is interrupted is

$$p_I = \int_0^{\Delta_O} x f_O(x) dx. \quad (33)$$

As one may observe, the duration of uninterrupted connectivity is produced by a geometrical distribution with the parameter p_I, which is scaled with the aggregate durations of non-outage and outage intervals conditioned on the event that it is smaller than Δ_O. Hence, we have

$$E[T_U] = \frac{1}{p_I} (E[G] + E[O|O \le \Delta_O]), \quad (34)$$

where the means are readily given by

$$E[G] = \int_0^\infty x f_G(x) dx, \ E[O|O \le \Delta_O] = \int_0^{\Delta_O} x \frac{f_O(x)}{1 - p_I} dx. \quad (35)$$

V. NUMERICAL RESULTS

In this section, the obtained analytical findings are illustrated, explained, and compared with the results produced with our SLS framework. Below is an illustrative example to demonstrate the capabilities of our proposed framework, which is applicable for a range of comprehensive and realistic deployment models currently under investigation.

We address a typical crowded urban deployment, where a pedestrian plaza (e.g., St. Peter's Square, Vatican City) is modeled. The area of interest is assumed to be of circular shape with the radius of 50 m. The terrestrial NR-BS is located at a side of the square on the wall of one of the buildings at the height of 10 m. Pedestrians move around the square by following their travel patterns as described in Section II with the fixed speed of 3 km/h. UAV-BSs are assumed to traverse the pedestrian plaza at the height of 20 m with the fixed speed that varies from 5 km/h to 40 km/h. The remaining modeling parameters are summarized in Table II. Our simulation parameters partially follow the guidelines in [24] with respect to the height and the speed of the UAV-BS, as well as refer to [11] for modeling the radio part.

To validate the assumptions of our developed analytical framework, we utilize an in-house SLS tool that incorporates all of the relevant procedures considered by our study. The mmWave-specific physical layer was designed by following the corresponding 3GPP guidelines; particularly, the 3GPP's 3D multipath channel model outlined in [11] was employed. This simulation tool captures the following key procedures: session arrival process, UAV-BS arrival and departure processes, UAV-BS and pedestrian mobility, and dynamic backhaul link rerouting between the UAV-BS and the NR-BS enhanced with multi-connectivity operation [38].

The tool operates in a time-driven manner with the step of 0.01 s. To match the capabilities of our analytical framework, idealistic and reliable signaling at all the connections has been assumed: if the current connection is interrupted, the COW-BS immediately attempts to reconnect via a UAV-BS and does not spend any additional resources for this migration. For the sake of better accuracy in the output results, all of the

TABLE II
DEPLOYMENT AND TECHNOLOGY PARAMETERS

| Parameter	Value
Deployment	
Area radius, R	50 m
Height of NR-BS, h_A	10 m
Height of UAV-BS, h_D	20 m
Height of COW-BS, h_C	1.5 m
Height of blocker, h_B	1.7 m
Radius of blocker, r_B	0.2 m
Speed of blocker, v	1 m/s
Technology	
NR-BS transmit power	35 dBm
UAV-BS transmit power	23 dBm
Target SNR for non-outage conditions	3 dB
COW-BS antenna gain	5 dB
UAV-BS antenna gain	7 dB
NR-BS antenna gain	10 dB
Carrier frequency	28 GHz
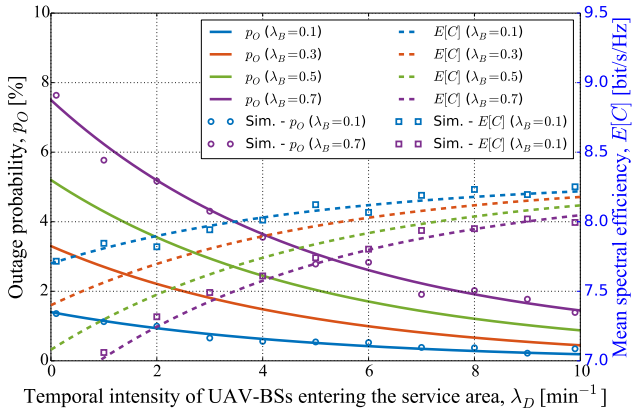
Fig. 5. Outage probability and mean spectral efficiency. Effect of crowd density and intensity of UAV-BS flights.

Fig. 7. Distribution of outage duration. Effect of UAV-BS speed and its capabilities.

collected intermediate data are averaged over 100 replications, each starting with a re-deployment of the layout. Each of such replications corresponds to 10 min of real-time operation. Hence, approximately 17 hours of real-time system operation have been modeled.

1) Effect of UAV-BS flight intensity: The UAV-BSs are assumed to move at a moderate speed of 10 km/h. The point 0 on the OX axis represents the baseline scenario with no UAV-BS assistance. Analyzing Fig. 5, we notice that both the outage probability and the spectral efficiency are improved with the growth in the intensity of UAV-BS traversals. Specifically, for $\lambda_B = 0.7$ the outage probability decreases from 7.5% for the baseline scenario to 1.5% for 10 UAV-BSs per minute. Meanwhile, the corresponding increase in the spectral efficiency is from 6.5 bit/s/Hz to 8 bit/s/Hz, which is around 25%.

Going further, we observe that the benefits of UAV-BS assistance for performance are more visible in challenging conditions (high density of humans, such as 0.7) rather than at low blocker densities (such as 0.1 or 0.3). Moreover, Fig. 5 clearly indicates that two UAV-BSs traversing the area of interest per minute with $\lambda_B = 0.7$ reduce the outage probability down to 5.3%, which is close to 5.2% observed with $\lambda_B = 0.5$ in the baseline scenario (no UAV-BSs, $\lambda_D = 0$).

We finally note that the results of our mathematical analysis match well with those obtained via the simulation tool, which confirms the accuracy of the analytical findings. A slight difference between them is due to several simplifying assumptions introduced by the mathematical framework for
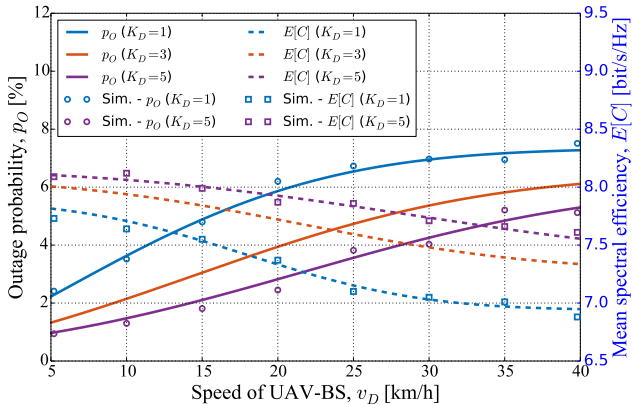
the sake of analytical tractability: e.g., an approximation of the 3GPP's multipath propagation model as detailed in Section III and [28].

2) Effect of UAV-BS flight speed: The intensity of UAV-BSs traversing the area, λ_D, is fixed and set to 10 UAV-BSs per min. We model a crowded scenario with $\lambda_B = 0.7$, while the maximum number of simultaneous backhaul connections per UAV-BS, K_D, varies from 1 to 5. We observe that a decrease in the UAV-BS speeds has a notable positive effect on performance. As an example, lowering UAV-BS speeds from 40 km/h down to 10 km/h for $K_D = 1$ results in reduced outage probability from 7.1% to 3.5%, which is over 2 times. The corresponding gain in the mean spectral efficiency, $E[C]$, is smaller but still visible: from 6.9 bit/s/Hz to 7.7 bit/s/Hz.

We continue by evaluating the effect of the UAV-BS speeds in Fig. 7, which presents the pdf of the outage duration for certain values of v_D and K_D. The UAV-BS intensity, λ_D, is set to 10 per min, while the density of humans in the area, λ_B, equals 0.7. There is a notable decrease in the mean outage duration, $E[O]$, when UAV-BSs are utilized. Particularly, the said parameter decreases from 276 ms for the baseline deployment down to as low as 88 ms for ($v_D = 10$ km/h, $K_D = 10$) case. Finally, we notice that increasing the UAV-BS capacity, K_D, by two times (from 5 to 10 simultaneous connections) brings a notable decrease in the mean outage duration.

3) Effect of service capacity of UAV-BSs, K_D: To this aim, we analyze the primary backhaul session continuity related parameter – the average duration of the uninterrupted connectivity subject to a certain tolerable outage duration. In other words, a connection is assumed to be interrupted if and only if the outage duration is longer than a certain value, Δ_O. We illustrate these results in Fig. 8 for two UAV-BS intensities ($\lambda_D = 1$ and 10 UAV-BSs per min).

Studying Fig. 8, we notice that for 100 ms of tolerable outage, the average duration of uninterrupted connectivity grows from 7 s for the baseline scenario to 46 s for 10 UAV-BSs per min, $K_D = 10$. We then observe that the impact of an increased UAV-BS capacity, K_D, is notable but weaker than that of the intensity of UAV-BS traversals: the curve for (10 UAV-BSs per min, $K_D = 1$) is much higher than the one for (1 UAV-BS per min, $K_D = 10$). This is mainly due to the fact that at least one out of 10 UAV-BSs is much more likely to reside in non-outage conditions with respect to the COW-BS than a single UAV-BS, regardless of the capacity.

Fig. 6. Outage probability and mean spectral efficiency. Effect of UAV-BS speed and its capabilities.
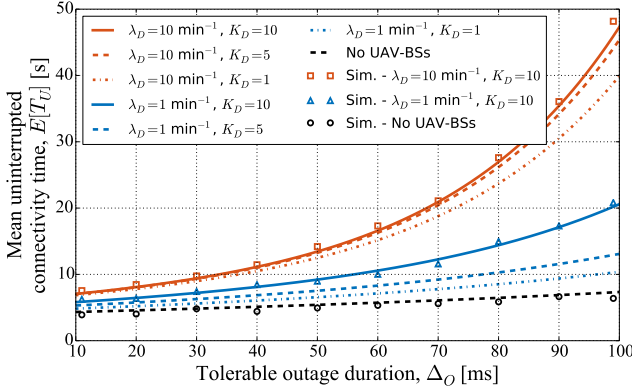
Fig. 8. Mean uninterrupted connectivity time. Effect of UAV-BS traversal intensity and its capabilities.

Finally, we observe that the relative impact of K_D on the said parameter depends on the intensity of UAV-BS flights across the area. Particularly, the improvement brought by $K_D = 5$ and $K_D = 10$ vs. $K_D = 1$ is significant for 1 UAV-BS per min and marginal for 10 UAV-BSs per min. In summary, for high intensity of UAV-BS traversals, there is no need for higher capacity of the UAV-BSs. Meanwhile, if the intensity of UAV-BS flights is lower than required from the connectivity perspective, there is a driver to invest resources into advanced radio units on the UAV-BSs.

VI. CONCLUSION

Dynamic and reconfigurable system architectures aiming to support backhaul operation in mmWave bands are one of the recent focus items in the ongoing 3GPP standardization. They can be further augmented by an emerging element in the 5G landscape – UAVs with flexible mobility and capability to carry radio equipment. These may become efficient backhaul connectivity providers in 5G and beyond networks, especially in case of highly dynamic traffic fluctuations to avoid excessive over-provisioning of network resources.

To this aim, we contribute a new analytical framework that incorporates 3GPP's multipath channel model, heterogeneous mobility of UAVs and humans, as well as human body blockage effects, which are identified by 3GPP as one of the main sources of performance degradation for the prospective NR operation. Our methodology allows to produce both time-averaged and continuous-time metrics in dependence on UAV-BS speed and traversal intensity, heights of the communicating entities within the scenario (NR-BS, UAV-BS, COW-BS, and human blockers), as well as blocker dimensions and speeds.

We demonstrate that UAV-BS assistance can offer significant benefits to mmWave backhaul under certain system parameters. For instance, the intensity of UAV-BS flights equal to 10 reduces the outage probability on a COW-BS backhaul link by 6 times. Moreover, by lowering the UAV-BS speed above the service area from 40 km/h down to 10 km/h, the said outage probability drops by 2 times. Further, one may derive the target intensity of UAV-BS traversals that is required to support the key performance indicators as a function of the blocker density. The contributed framework can be applied to a wide range of practical scenarios, such as conventional layouts with the near-static deployment of UAV-BSs by e.g., adjusting the speed parameter.

REFERENCES

[1] M. Shafi, A. F. Molisch, P. J. Smith, T. Haustein, P. Zhu, P. D. Silva, F. Tufvesson, A. Benjebbour, and G. Wunder, "5G: A Tutorial Overview of Standards, Trials, Challenges, Deployment, and Practice," *IEEE Journal on Selected Areas in Communications*, vol. 35, no. 6, pp. 1201–1221, June 2017.

[2] 5GPPP, "View on 5G Architecture," White paper v2.0, December 2017.

[3] 3GPP, "Report of 3GPP TSG RAN meeting #78," 3GPP RP-180516, December 2017.

[4] J. Sachs, G. Wikstrom, T. Dudda, R. Baldemair, and K. Kittichokechai, "5G Radio Network Design for Ultra-Reliable Low-Latency Communication," *IEEE Network*, vol. 32, no. 2, pp. 24–31, March 2018.

[5] U. Siddique, H. Tabassum, E. Hossain, and D. I. Kim, "Wireless backhauling of 5G small cells: Challenges and solution approaches," *IEEE Wireless Communications*, vol. 22, no. 5, pp. 22–31, October 2015.

[6] C. Dehos, J. L. Gonzalez, A. D. Domenico, D. Ktenas, and L. Dussopt, "Millimeter-wave access and backhauling: The solution to the exponential data traffic increase in 5G mobile communications systems?" *IEEE Communications Magazine*, vol. 52, no. 9, pp. 88–95, September 2014.

[7] T. Bai, R. Vaze, and R. W. Heath, "Analysis of blockage effects on urban cellular networks," *IEEE Transactions on Wireless Communications*, vol. 13, no. 9, pp. 5070–5083, September 2014.

[8] M. Gapeyenko *et al.*, "On the temporal effects of mobile blockers in urban millimeter-wave cellular scenarios," *IEEE Transactions on Vehicular Technology*, vol. 66, no. 11, pp. 10 124–10 138, November 2017.

[9] V. Petrov, M. Komarov, D. Moltchanov, J. M. Jornet, and Y. Koucheryavy, "Interference and SINR in Millimeter Wave and Terahertz Communication Systems With Blocking and Directional Antennas," *IEEE Transactions on Wireless Communications*, vol. 16, no. 3, pp. 1791–1808, March 2017.

[10] V. Petrov, M. A. Lema, M. Gapeyenko, K. Antonakoglou, D. Moltchanov, F. Sardis, A. Samuylov, S. Andreev, Y. Koucheryavy, and M. Dohler, "Achieving End-to-End Reliability of Mission-Critical Traffic in Softwarized 5G Networks," *IEEE Journal on Selected Areas in Communications*, vol. 36, no. 3, pp. 485–501, March 2018.

[11] 3GPP, "Study on channel model for frequencies from 0.5 to 100 GHz (Release 15)," 3GPP TR 38.901 V15.0.0, June 2018.

[12] F. B. Tesema, A. Awada, I. Viering, M. Simsek, and G. Fettweis, "Evaluation of context-aware mobility robustness optimization and multi-connectivity in intra-frequency 5G ultra dense networks," *IEEE Wireless Communications Letters*, vol. 5, no. 6, pp. 608–611, December 2016.

[13] O. E. Ayach, S. Subramanian, J. E. Smee, A. Sampath, and J. Li, "Method and apparatus for connection point discovery and association in a directional wireless network," October 2016, US9474013B2. [Online]. Available: https://patents.google.com/patent/US9474013B2/en

[14] M. Mousaei and B. Smida, "Optimizing pilot overhead for ultra-reliable short-packet transmission," in *IEEE International Conference on Communications*, May 2017.

[15] NGMN, "Small cell backhaul requirements," White paper, June 2012.

[16] 3GPP, "Study on integrated access and backhaul (Release 15)," 3GPP TR 38.874 V0.4.0, August 2018.

[17] C. Saha, M. Afshang, and H. S. Dhillon, "Integrated mmWave Access and Backhaul in 5G: Bandwidth partitioning and downlink analysis," *Available: https://arxiv.org/pdf/1710.06255.pdf*, 2018.

[18] K. Balachandran, J. Kang, K. Karakayali, and J. Singh, "Capacity benefits of relays with in-band backhauling in cellular networks," in *IEEE International Conference on Communications*, May 2008.

[19] M. Jaber, F. J. Lopez-Martinez, M. A. Imran, A. Sutton, A. Tukmanov, and R. Tafazolli, "Wireless backhaul: Performance modelling and impact on user association for 5G," *IEEE Transactions on Wireless Communications*, pp. 1–1, 2018.

[20] I. Bor-Yaliniz, A. El-Keyi, and H. Yanikomeroglu, "Efficient 3-D placement of an aerial base station in next generation cellular networks," in *IEEE International Conference on Communications*, May 2016.

[21] E. Kalantari, M. Z. Shakir, H. Yanikomeroglu, and A. Yongacoglu, "Backhaul-aware robust 3D drone placement in 5G+ wireless networks," in *IEEE International Conference on Communications Workshops (ICC Wkshps)*, May 2017, pp. 1–6.

[22] M. Mozaffari, W. Saad, M. Bennis, and M. Debbah, "Efficient deployment of multiple unmanned aerial vehicles for optimal wireless coverage," *IEEE Communications Letters*, vol. 20, no. 8, pp. 1647–1650, August 2016.

[23] K. Haneda *et al.*, "5G 3GPP-like channel models for outdoor urban microcellular and macrocellular environments," in *IEEE 83rd Vehicular Technology Conference (VTC Spring)*, May 2016.

[24] 3GPP, "Study on enhanced LTE support for aerial vehicles, (Release 15)," TR 36.777 V15.0.0, January 2018.

[25] A. Fotouhi, M. Ding, and M. Hassan, "Dynamic base station repositioning to improve performance of drone small cells," in *2016 IEEE Globecom Workshops (GC Wkshps)*, December 2016, pp. 1–6.

[26] J. G. Andrews, T. Bai, M. Kulkarni, A. Alkhateeb, A. Gupta, and R. W. Heath, "Modeling and analyzing millimeter wave cellular systems," *IEEE Transactions on Communications*, vol. 65, no. 1, pp. 403–430, January 2016.

[27] M. Zhang, M. Polese, M. Mezzavilla, S. Rangan, and M. Zorzi, "Ns-3 Implementation of the 3GPP MIMO Channel Model for Frequency Spectrum above 6 GHz," in *Workshop on ns-3*, June 2017.

[28] M. Gapeyenko, V. Petrov, D. Moltchanov, S. Andreev, Y. Koucheryavy, M. Valkama, M. R. Akdeniz, and N. Himayat, "An Analytical Representation of the 3GPP 3D Channel Model Parameters for mmWave Bands," in *2nd ACM Workshop on Millimeter-Wave Networks and Sensing Systems*, October 2018, pp. 1–6.

[29] Y. Zeng, R. Zhang, and T. J. Lim, "Wireless communications with unmanned aerial vehicles: Opportunities and challenges," *IEEE Communications Magazine*, vol. 54, no. 5, pp. 36–42, May 2016.

[30] P. Nain, D. Towsley, B. Liu, and Z. Liu, "Properties of random direction models," in *IEEE INFOCOM*, vol. 3, March 2005.

[31] A. M. Mathai, *An introduction to geometrical probability: Distributional aspects with applications*. CRC Press, 1999, vol. 1.

[32] G. Newell, "The M/G/∞ queue," *SIAM Journal on Applied Mathematics*, vol. 14, no. 1, pp. 86–88, 1966.

[33] R. Groenevelt, "Stochastic models for mobile ad hoc networks," INRIA Sophia-Antipolis, PhD thesis, 2005.

[34] D. J. Daley, "The busy period of the M/GI/∞ queue," *Queueing Systems: Theory and Applications*, vol. 38, no. 2, pp. 195–204, 2001.

[35] J. G. Kemeny, J. L. Snell *et al.*, *Finite Markov chains*. van Nostrand Princeton, NJ, 1960, vol. 356.

[36] T. Altiok, "On the phase-type approximations of general distributions," *IIE Transactions*, vol. 17, no. 2, pp. 110–116, 1985.

[37] M. F. Neuts, *Matrix-geometric solutions in stochastic models: an algorithmic approach*. Courier Corporation, 1981.

[38] V. Petrov *et al.*, "Dynamic multi-connectivity performance in ultra-dense urban mmWave deployments," *IEEE Journal on Selected Areas in Communications*, vol. 35, no. 9, pp. 2038–2055, September 2017.

Dmitri Moltchanov (dmitri.moltchanov@tut.fi) is a Senior Research Scientist in the Laboratory of Electronics and Communications Engineering, Tampere University of Technology, Finland. He received his M.Sc. and Cand.Sc. degrees from Saint-Petersburg State University of Telecommunications, Russia, in 2000 and 2002, respectively, and Ph.D. degree from Tampere University of Technology in 2006. His research interests include performance evaluation and optimization issues of wired and wireless IP networks, Internet traffic dynamics, quality of user experience of real-time applications, and traffic localization P2P networks. Dmitri Moltchanov serves as TPC member in a number of international conferences. He authored more than 50 publications.

Sergey Andreev (sergey.andreev@tut.fi) received the Specialist and Cand.Sc. degrees from St. Petersburg State University of Aerospace Instrumentation, St. Petersburg, Russia, in 2006 and 2009, respectively, and the Ph.D. degree from Tampere University of Technology, Finland, in 2012. Since 2018, he has been a Visiting Senior Research Fellow with the Centre for Telecommunications Research, Kings College London, U.K. He is currently a Senior Research Scientist with the Laboratory of Electronics and Communications Engineering, Tampere University of Technology. He has authored or co-authored over 150 published research works on wireless communications, energy efficiency, heterogeneous networking, cooperative communications, and machine-to-machine applications.

Margarita Gapeyenko (margarita.gapeyenko@tut.fi) is a Ph.D. candidate at the Laboratory of Electronics and Communications Engineering at Tampere University of Technology, Finland. She earned her M.Sc. degree in Telecommunication Engineering from University of Vaasa, Finland, in 2014, and B.Sc. degree in Radio-Engineering, Electronics, and Telecommunications from Karaganda State Technical University, Kazakhstan, in 2012. Her research interests include mathematical analysis, performance evaluation, and optimization methods for mmWave networks, UAV communications, and (beyond-)5G heterogeneous systems.

Nageen Himayat is a Principal Engineer with Intel Labs, where she leads a team conducting research on several aspects of next generation (5G/5G+) of mobile broadband systems. Her research contributions span areas such as multi-radio heterogeneous networks, mm-wave communication, energy-efficient designs, cross layer radio resource management, multi-antenna, and non-linear signal processing techniques. She has authored over 250 technical publications, contributing to several IEEE peer-reviewed publications, 3GPP/IEEE standards, as well as holds numerous patents. Prior to Intel, Dr. Himayat was with Lucent Technologies and General Instrument Corp, where she developed standards and systems for both wireless and wire-line broadband access networks. Dr. Himayat obtained her B.S.E.E degree from Rice University, and her Ph.D. degree from the University of Pennsylvania. She also holds an MBA degree from the Haas School of Business at University of California, Berkeley.

Vitaly Petrov (vitaly.petrov@tut.fi) received the M.Sc. degree in information systems security from the Saint Petersburg State University of Aerospace Instrumentation, St Petersburg, Russia, in 2011, and the M.Sc. degree in communications engineering from the Tampere University of Technology, Tampere, Finland, in 2014, where he is currently pursuing the Ph.D. degree. He was a Visiting Scholar with the Georgia Institute of Technology, Atlanta, USA, in 2014 and a Strategic Intern with the Nokia Research Center, Helsinki, Finland, in 2012. He is the recipient of Best Student Paper Award at IEEE VTC-Fall'15 and Best Student Poster Award at IEEE WCNC'17. His current research interests are in Internet-of-Things, mmWave/THz band communications, nanonetworks, cryptology, and network security.

Yevgeni Koucheryavy (evgeni.koucheryavy@tut.fi) received the Ph.D. degree from the Tampere University of Technology, in 2004. He is a Professor with the Laboratory of Electronics and Communications Engineering, Tampere University of Technology, Finland. He is the author of numerous publications in the field of advanced wired and wireless networking and communications. His current research interests include various aspects in heterogeneous wireless communication networks and systems, the Internet of Things and its standardization, and nanocommunications. He is an Associate Technical Editor of the IEEE Communications Magazine and Editor of the IEEE Communications Surveys and Tutorials.